48
8-15-95 JS 2

PREPARED FOR THE U.S. DEPARTMENT OF ENERGY,
UNDER CONTRACT DE-AC02-76-CHO-3073

PPPL-3117
UC-420,426

PPPL-3117

IMPROVED CONFINEMENT WITH REVERSED MAGNETIC SHEAR IN TFTR

BY

F.M. LEVINTON, M.C. ZARNSTORFF, S.H. BATHA, ET AL.

JULY 1995

PPPL PRINCETON PLASMA PHYSICS LABORATORY

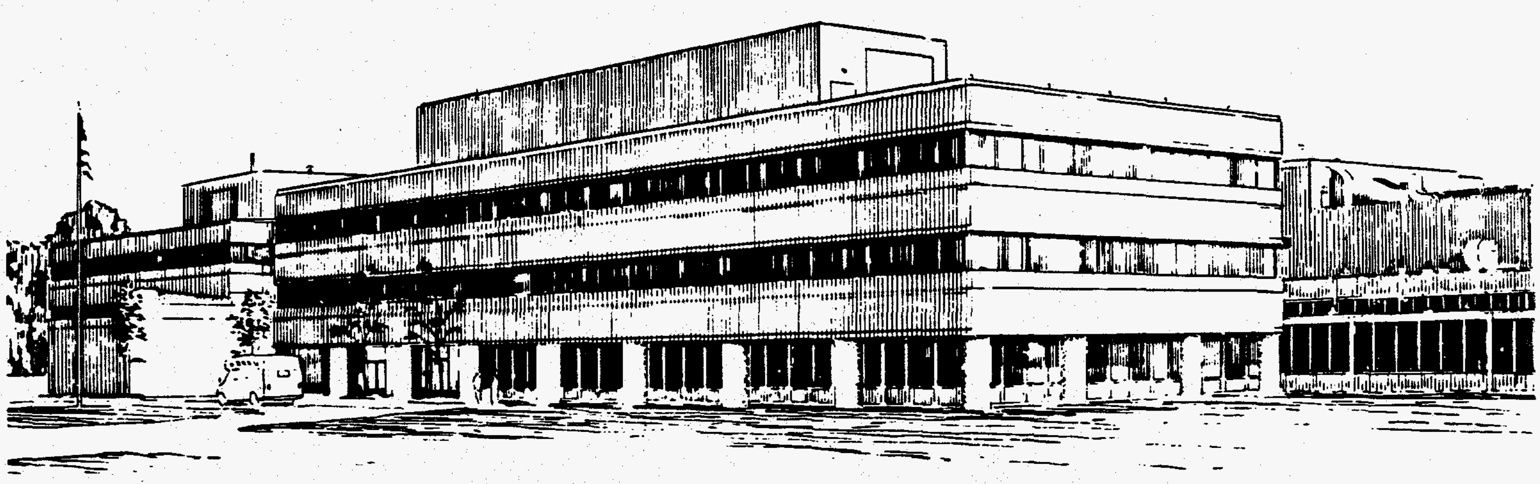

PRINCETON UNIVERSITY, PRINCETON, NEW JERSEY

DISCLAIMER

Improved Confinement with Reversed Magnetic Shear in TFTR

F. M. Levinton[1], M. C. Zarnstorff[2], S. H. Batha[1], M. Bell[2], R. E. Bell[2], R. V. Budny[2], C. Bush[3], Z. Chang[2], E. Fredrickson[2], A. Janos[2], H. Park[2], A. Ramsey[2], G. L. Schmidt[2], E. Synakowski[2], G. Taylor[2]

[1]*Fusion Physics and Technology, Torrance, CA 90503*

[2]*Princeton Plasma Physics Laboratory, P.O. Box 451, Princeton, NJ 08543*

[3]*Oak Ridge National Laboratory, Oak Ridge, TN 37831*

(June 7, 1995)

Abstract

Highly peaked density and pressure profiles in a new operating regime have been observed on the Tokamak Fusion Test Reactor (TFTR). The q-profile has a region of reversed magnetic shear extending from the magnetic axis to $r/a \sim 0.3-0.4$. The central electron density rises from $0.45 \times 10^{20}\,\mathrm{m}^{-3}$ to nearly $1.2 \times 10^{20}\,\mathrm{m}^{-3}$ during neutral beam injection. The electron particle diffusivity drops precipitously in the plasma core with the onset of the improved confinement mode and can be reduced by a factor of ~ 50 to near the neoclassical particle diffusivity level.

52.55.-s, 52.55.Fa, 52.30.Bt

Typeset using REVTEX

The economic attractiveness of the tokamak as a candidate for a fusion reactor depends on development of a magnetic configuration that has good confinement, stability, and low recirculating power for steady state current drive. This requires a high fraction of self-sustaining bootstrap current that is well aligned with an optimized current density profile for confinement and stability. Recent studies [1] of the optimization of the current density profile suggest that reversed magnetic shear (i.e. a hollow current density profile), is desirable for confinement, stability, and bootstrap alignment. Shear is defined as, $s \equiv (2V/q)(dq/d\psi)(d\psi/dV) \approx (r/q)(dq/dr)$, where ψ is the enclosed poloidal flux, V is the enclosed volume, q is the safety factor and r is the minor radius. Shear is thought to be important because it can stabilize some classes of microinstabilities such as trapped electron modes [2], a candidate to explain the observed anomalous electron transport in tokamaks. Reversed magnetic shear can also stabilize some magnetohydrodynamic (MHD) instabilities such as ballooning modes [3] and resistive tearing modes. A further benefit, if improved core confinement can be attained, is a high pressure gradient that would generate a strong off-axis bootstrap current, and sustain the hollow current density profile. This scenario may lead to an attractive concept for a steady state tokamak reactor [4]. Most tokamaks operate with inductive current drive which will normally produce peaked current density profiles at the magnetic axis due to the strong dependence of the plasma conductivity on the electron temperature. Only by non-inductive current drive or transient techniques can a hollow current density profile be generated. This has been done in several experiments such as Tore-Supra [5] using lower hybrid current drive (LHCD) and JET [6,7] using pellet injection. These experiments have reported improved performance that could be attributed to reversed shear.

Recent experiments on the Tokamak Fusion Test Reactor (TFTR) [8] have demonstrated a reversed shear configuration. With measurements of $q(R,t)$ from the motional Stark effect (MSE) [9,10] diagnostic providing good temporal and spatial resolution, a correlation of the effect of magnetic shear on improved transport and stability has been observed and will be reported in this Letter. Two different discharge startup scenarios have been developed to produce q-profiles with reversed magnetic shear. Both have improved electron particle and thermal diffusivity. In both cases the plasma is initially started at or near full size and ramped up in current at a ramp rate of 1.8 MA/s to about 1.0 MA. For one scenario the rate of rise of the plasma current is reduced to 0.4 MA/s until the final plasma current of $I_p = 1.6$ MA is reached, as shown in Fig. 1(a). Having a large plasma, while the current is still low and rising, forces the current to form initially at the edge and to diffuse towards the center. Since the current diffusion time is much longer than the rise time of the plasma current, a hollow current density profile is formed. To further slow down the current penetration to the plasma center, neutral beam injection (NBI) begins with a low power "prelude" phase at ~ 0.6 seconds, with 5-7.5 MW of power injected into the plasma. This is followed by the main heating phase with up to 25 MW of NBI, as shown in Fig. 1(a). The prelude phase causes the electron temperature to increase from $\sim$ 2 keV to $\sim$ 5 keV, making the current diffusion time $\sim$ 10 seconds. Neutral beam injection, co-tangential to the plasma current, is used in the early phase to drive a significant fraction of the plasma current and further slow the poloidal flux diffusion. Typical q-profiles for this evolution, shown in Fig. 2, have been reconstructed with the VMEC equilibrium code [11] from the MSE data, kinetic pressure data, calculated fast ion pressure from the TRANSP code [12], and external magnetics data. The uncertainties in $q(R)$ are 10% or less across the profile [13]. The q-profile has $q(0) \geq 4 - 5$ and $q_{min} \sim 3$ at $t = 2.0\,s$. Both $q(0)$ and q_{min} slowly decrease on a time scale of several seconds and reach $q(0) \sim 3 - 4$ and $q_{min} \sim 2$ after three seconds of beam heating, consistent with the neoclassical current diffusion rate. This allows for considerable experimental flexibility to determine the target values for $q(0)$ and q_{min} in the main heating phase of the discharge.

The plasmas formed in the reversed shear configuration, both in the prelude and heating phase, behave as typical supershots [14] at this power, with a central ion temperature of $\sim$ 20 keV, electron temperature of $\sim 6 - 7$ keV and a central electron density of $\sim 4 \times 10^{19}\,\mathrm{m}^{-3}$. However, above a threshold in neutral beam power, in the range of $\sim$ 18-25 MW, the particle and thermal transport dramatically improves in the plasma core where the shear is reversed. The effect is most strongly seen on the particle diffusivity. The central electron density increases from $\sim 4 \times 10^{19}\ \mathrm{m}^{-3}$ to $\sim 1.2 \times 10^{20}\,\mathrm{m}^{-3}$ in $\sim$ 0.3 seconds, as measured by a 10-channel interferometer array and shown in Fig. 3(a). The density profile outside the reversed shear region changes little, resulting in a peaked density profile. The transition from a normal supershot to the highly peaked reversed shear mode, "R/S-mode", occurs abruptly during the discharge, usually 0.2-0.3 seconds after the start of the main heating phase. Shown in Fig. 4, is the evolution of the central density, with a transition into the R/S-mode at $t = 2.715$ s. In a preceding discharge, with a similar reversed shear q-profile, but lower NBI power, the density saturates by 2.7 seconds and no transition occurs, as shown in Fig. 4. In both discharges the main heating phase starts at 2.5 seconds, with the neutral beam power increasing from 7 MW to 19 MW in the plasma that does not exhibit a transition into the R/S-mode and to 25 MW in the plasma which does. In both cases the NBI is near balanced with little measured plasma rotation. The electron and ion temperature profiles also change when the plasma makes the transition into the R/S-mode. The electron temperature increases $\sim 25\%$ in the core region only, with little change outside, whereas the ion temperature profile is broadened. The resulting pressure profile, including the calculated fast ion contribution, shown in Fig. 3(b), is very peaked with a peaking factor, $F_p = p(0)/ < p >= 7.4$, where $p(0)$ is the pressure at the magnetic axis and $< p >$ is the volume-averaged pressure. This is larger than the typical peaking factors for supershots of ~ 5 and for L-mode discharges of ~ 3.3. We do not have q-profile measurements for these two discharges as the MSE measurements were obscured during the heating phase. However, at the end of the prelude phase the measured q-profiles are similar to those shown in Fig. 2.

The second scenario developed for reversed shear configurations on TFTR maintains a constant plasma current at 1.0 MA for one second after the initial current rise, before completing the current ramp up to 1.8 MA, as shown in Fig.1(b). This allows more current density to reach the plasma core and reduces $q(0)$ to 1.5-2.0. A prelude phase with 9 MW of NBI begins at 2.5 s before the main heating phase, with 16 MW, begins at 3.5 seconds. This case has several features that make it well suited for studying the effect of reversed shear on transport. The q-profile initially starts out monotonic with $q(0) \sim 1.5$. With the onset of the heating phase $q(0)$ rises and becomes non-monotonic at about 3.7 s. The final value for $q(0)$ is 2.3 and for q_{min} it is 1.8 after 0.8 seconds. The q_{min} radius starts near the magnetic axis and propagates outward for 0.5 s to $\rho = r/a \sim 0.3$, where a is the plasma minor radius. Coincident with the shear becoming negative, the electron density and temperature begin to increase rapidly. As in the earlier scenario, the electron density increase is significantly greater than the increase in electron temperature. This increase of electron pressure begins at ~ 3.85 s, near the magnetic axis, at about the time the shear becomes negative, and propagates outward in time, in a similar fashion to the reversed shear region. Shown in Fig. 5 is the electron pressure evolution at several minor radii. The initial rise in the pressure, due to the additional NBI power starting at 3.5 seconds, saturates by 3.8 seconds for the companion discharge that does not have reversed shear. The time of the transition to the R/S-mode for each radial location is indicated by an arrow in Fig. 5 . The location nearest the magnetic axis, at $\rho = 0.05$, has a transition into the R/S-mode at ~ 3.85 seconds. At radial locations further from the axis there is an increasing delay before the electron pressure begins to increase. Beyond $\rho \sim 0.45$ no change in pressure is observed. Shown in Fig. 6 is the shear evolution at several minor radii. Also indicated in Fig. 6 for each value of ρ is the time at which the improved confinement is observed, such as shown in Fig. 5 for the electron pressure evolution. The increase in the electron density and temperature occurs after the shear has been reduced and not only in the region of reversed shear, but extending into the region of reduced positive shear. The relation between reversed shear and improved transport is not a simple one, as it appears that the threshold in shear varies across the plasma minor radius due to some additional underlying dependencies. In the region beyond $\rho \sim 0.45$ no reduction of shear is measured and no improvement in transport is observed.

The transport analysis using the TRANSP code, from this and previous data, shows that the particle diffusivity drops precipitously in the region of reversed and reduced shear when the R/S-mode begins. The inferred particle diffusivity, assuming no pinch terms, can drop by as much as a factor of 50 from $D_e \sim 0.25\, m^2/s$ to near the neoclassical level of $D_e \sim 0.005\, m^2/s$ in the reversed shear region. There is a reduction of a factor of 2-3 in the ion and electron thermal diffusivity, but not in all discharges. It is not yet apparent what determines the threshold in the magnetic shear or, as in the previous scenario, the injected neutral beam power. Reversed shear appears to be a necessary, but not sufficient condition for the R/S-mode.

The reversed shear plasmas are observed to be free of any coherent, low-n or high-n MHD activity in the region of reversed shear. This includes the discharges with very peaked pressure profiles, and large pressure gradients, $p' = dp/d\psi$, which are often the driving mechanism for MHD instabilities. The pressure gradient, p' in the R/S-mode is larger, by a factor of 3-5 than typical TFTR supershots, which often have low-n MHD modes in the plasma core. They are believed to be neoclassical tearing modes [15], which theoretically may be stabilized by reversed shear. Outside the region of reversed shear MHD modes are sometimes present and are currently limiting the stability and performance of the R/S-mode to values of $\beta_N^* = 3.1$, where $\beta^* \equiv 2\mu_0 < p^2 >^{1/2} / B_T^2$ and $\beta_N^* = \beta^* a B_T / I_p(MA)$, with B_T the vacuum toroidal field, in Tesla. The discharges with high performance develop low-n MHD modes and possibly a ballooning mode just outside the q_{min} radius before terminating in a disruption. The exact cause of the disruption is not yet certain and is a subject of ongoing investigation.

In conclusion, highly peaked density and pressure profiles in a new operating regime have been observed on TFTR with a reversed magnetic shear configuration that reduces particle transport by over an order of magnitude to near neoclassical levels. The improved transport is in the region of reversed shear and extends out to the reduced shear region as well. With variations of the neutral beam prelude timing, heating phase timing, and total current, a range of reversed shear configurations has been produced. The safety factor on axis is in the range from $2-5$ and q_{min} varies from $1.8-3$. We expect to further extend the range of $q(0)$ and q_{min}. The stability limit has been tested in only two scenarios to date. According to ideal MHD theory the β_N^* limit is sensitive to the value of q_{min}, $q(0)$, and the total plasma current. With further optimization we hope to extend the β_N^* limit beyond the present value of 3.1 making the R/S-mode an attractive paradigm for an advanced tokamak reactor.

We would like to thank the TFTR staff for their support and operation of the experiment. This work was supported by United States Department of Energy Contract No. DE-AC02-76-CHO-3073.

REFERENCES

[1] C. Kessel, J. Manickam, G. Rewoldt, and W. M. Tang, Phys. Rev. Lett. **72**, 1212 (1994).

[2] B. B. Kadomtsev and O. P. Pogutse, Soviet Physics JETP **24**, 1172 (1967).

[3] A. Sykes, J. A. Wesson, and S. J. Cox, Phys. Rev. Lett. **39**, 757 (1977).

[4] R. J. Goldston *et al.*, Plasma Physics and Controlled Fusion **36**, B213 (1994).

[5] D. Moreau *et al.*, *Plasma Physics and Controlled Nuclear Fusion Research, Würzburg, 1992* (International Atomic Energy Agency, Vienna, 1993), Vol. I, p. 649.

[6] G. L. Schmidt *et al.*, *Plasma Physics and Controlled Nuclear Fusion Research, Nice, 1988* (International Atomic Energy Agency, Vienna, 1989), Vol. I, p. 215.

[7] M. Hugon *et al.*, Nucl. Fusion **32**, 33 (1992).

[8] D. M. Meade and the TFTR group, *Plasma Physics and Controlled Nuclear Fusion Research, Washington, D. C. 1990* (International Atomic Energy Agency, Vienna, 1991), Vol. I, pp. 9–24.

[9] F. M. Levinton *et al.*, Phys. Rev. Lett. **63**, 2060 (1989).

[10] F. M. Levinton, Rev. Sci. Instrum. **63**, 5157 (1992).

[11] S. P. Hirshman *et al.*, Phys. Plasmas **1**, 2277 (1994).

[12] R. J. Hawryluk, *Proc. Course in Physics of Plasmas Close to Thermonuclear Conditions, Varenna 1979* (CEC, Brussels, 1980), Vol. I, p. 19.

[13] S. H. Batha *et al.*, Submitted for publication .

[14] J. D. Strachan *et al.*, Phys. Rev. Lett. **58**, 1004 (1987).

[15] Z. Chang *et al.*, Nucl. Fusion **34**, 1309 (1994).

FIGURES

FIG. 1. The plasma current and neutral beam evolution for (a)the first scenario and (b)the second scenario.

FIG. 2. The q-profiles at the beginning of the current flatop at t=2 s (dashed line), and near the end of the heating phase at t=3.35 s (solid line) for the first scenario. The profiles are reconstucted by the VMEC equilibrium code and MSE data points are shown at t=3.35 s.

FIG. 3. The (a)density and (b)pressure profile before the transition to the R/S-mode (dashed line) and at the time of peak density and pressure (solid line).

FIG. 4. The evolution of the electron density at the magnetic axis for a discharge that makes a transition into the R/S-mode at 2.715 s (solid line) and a similar discharge at lower NBI power which does not (dashed line).

FIG. 5. The evolution of the electron pressure at several radial locations for a reversed shear discharge (solid line) and a companion non-reversed shear discharge (dashed line). The onset time of the improved confinement for the reversed shear discharge is indicated with an arrow for each radius.

FIG. 6. The evolution of the shear at several radial locations. The uncertainty of the shear is determined from many runs of the VMEC code with variations of the data within one standard deviation. The onset time of the improved confinement is indicated for each curve.

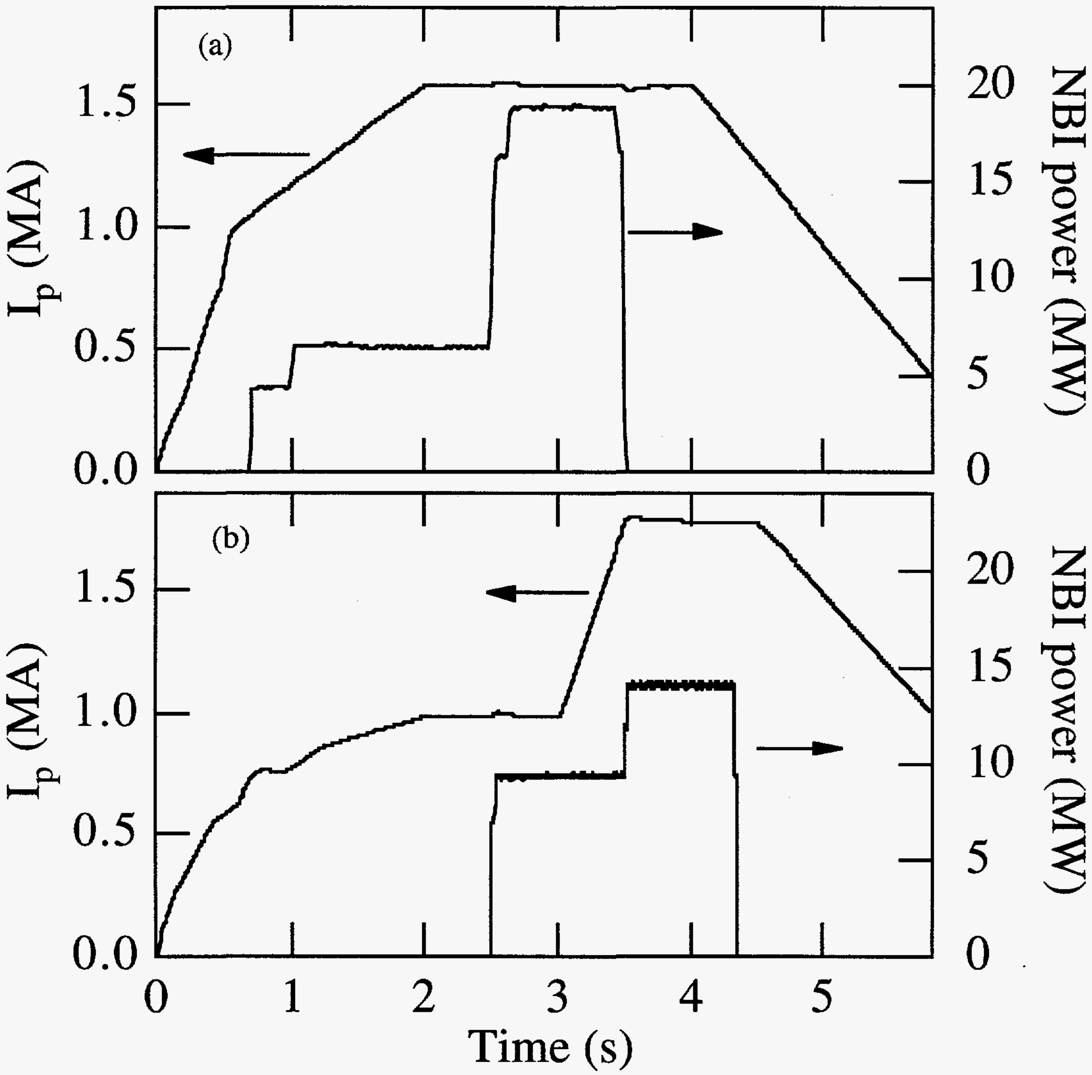

Figure 1.

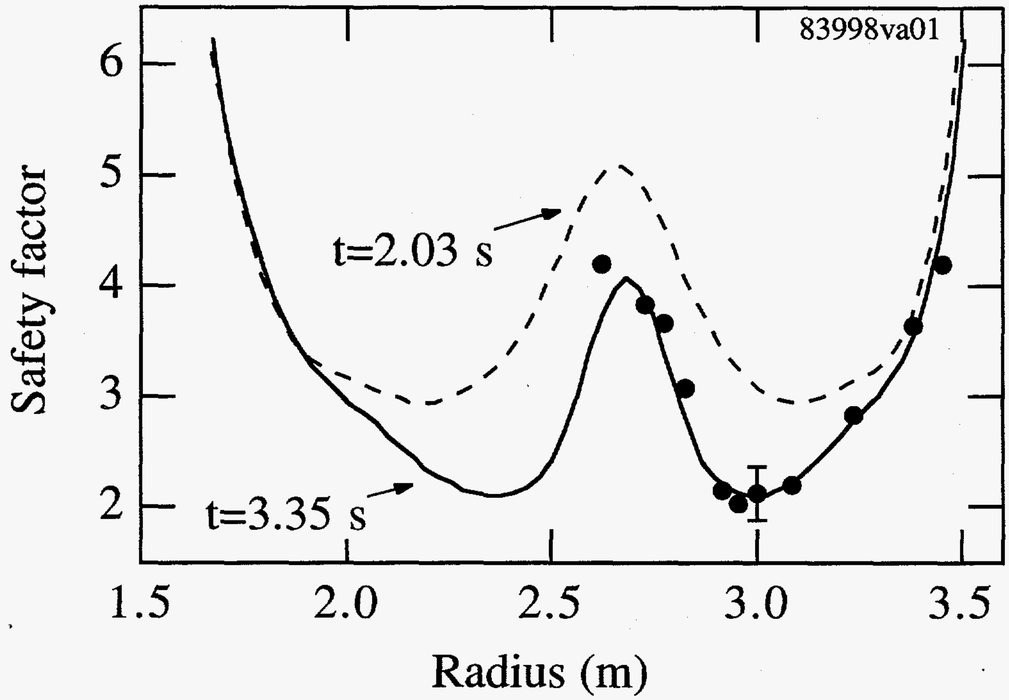
83998va01
6
5
4
3
2
Safety factor
t=2.03 s
t=3.35 s
1.5
2.0
2.5
3.0
3.5
Radius (m)

Figure 2.

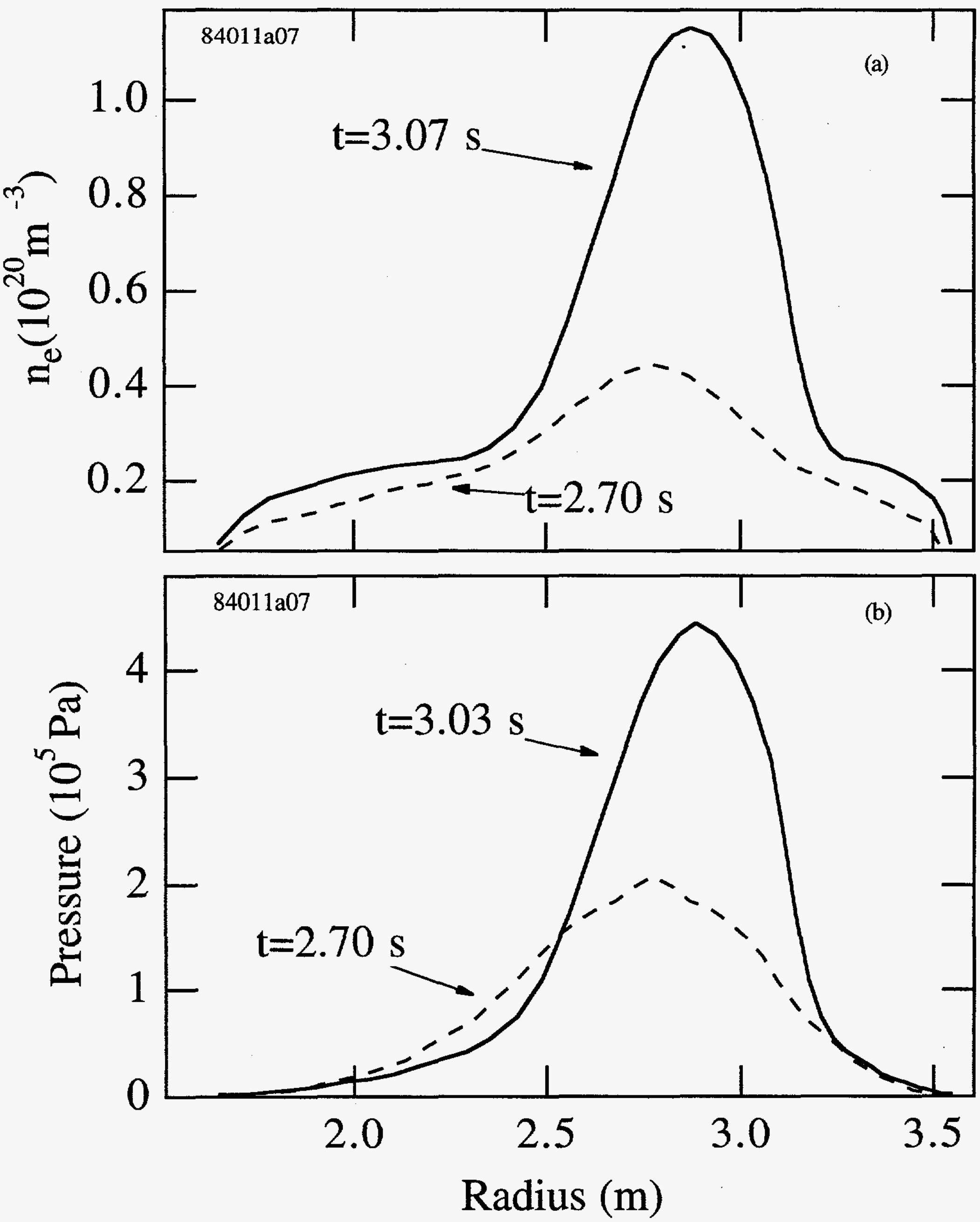
84011a07
(a)
$n_e(10^{20} m^{-3})$
1.0
0.8
0.6
0.4
0.2
t=3.07 s
t=2.70 s
84011a07
(b)
Pressure (10^5 Pa)
4
3
2
1
0
t=3.03 s
t=2.70 s
2.0
2.5
3.0
3.5
Radius (m)

Figure 3.

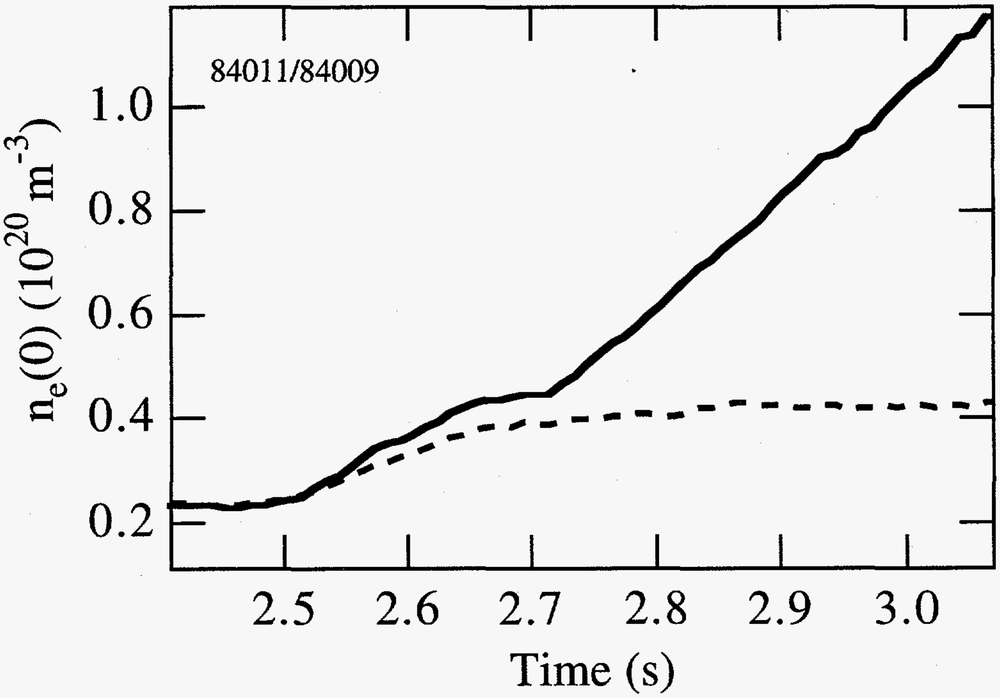

Figure 4.

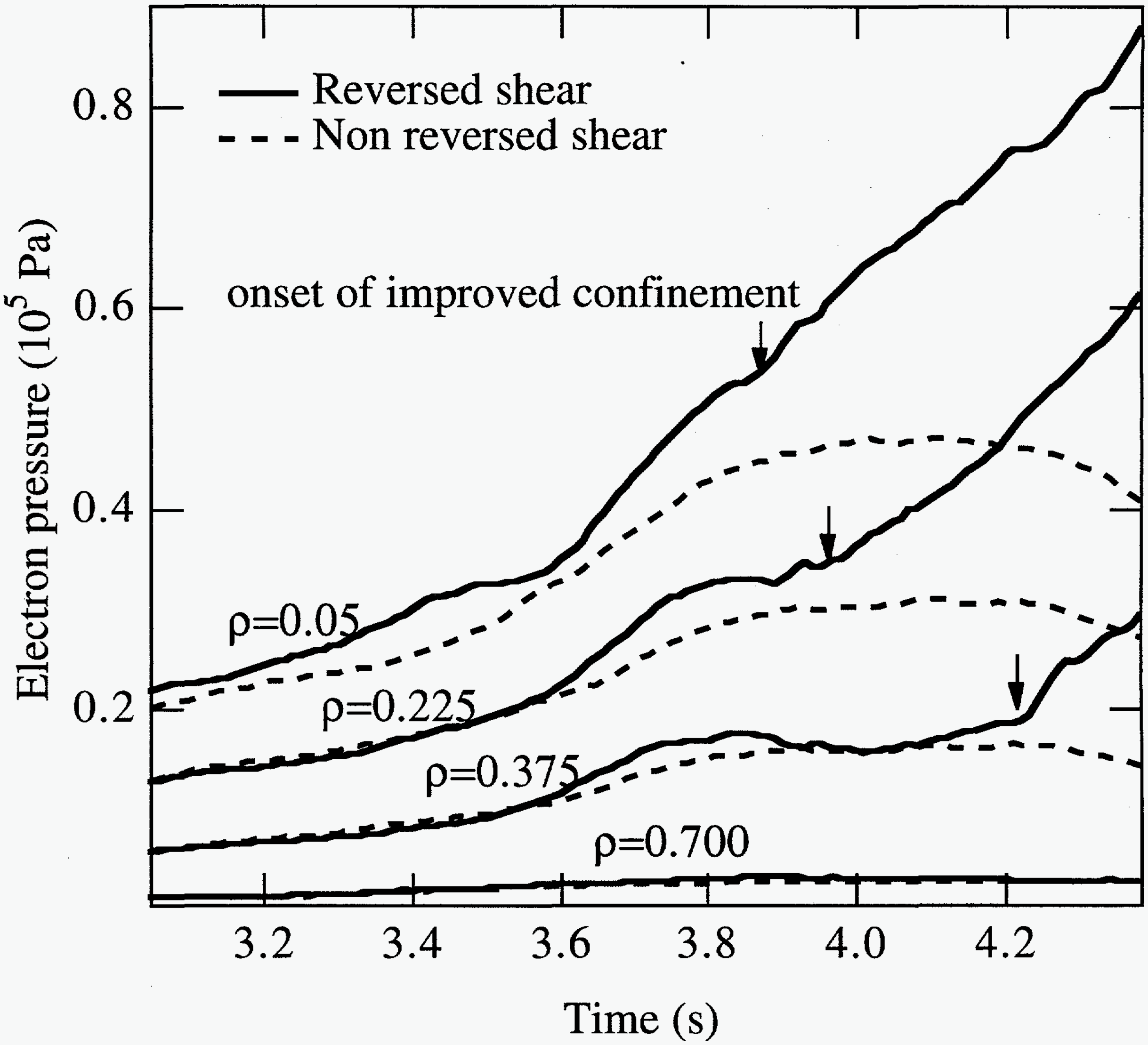

Reversed shear
Non reversed shear
onset of improved confinement
ρ=0.05
ρ=0.225
ρ=0.375
ρ=0.700
0.8
0.6
0.4
0.2
Electron pressure (10^5 Pa)
3.2
3.4
3.6
3.8
4.0
4.2
Time (s)

Figure 5.

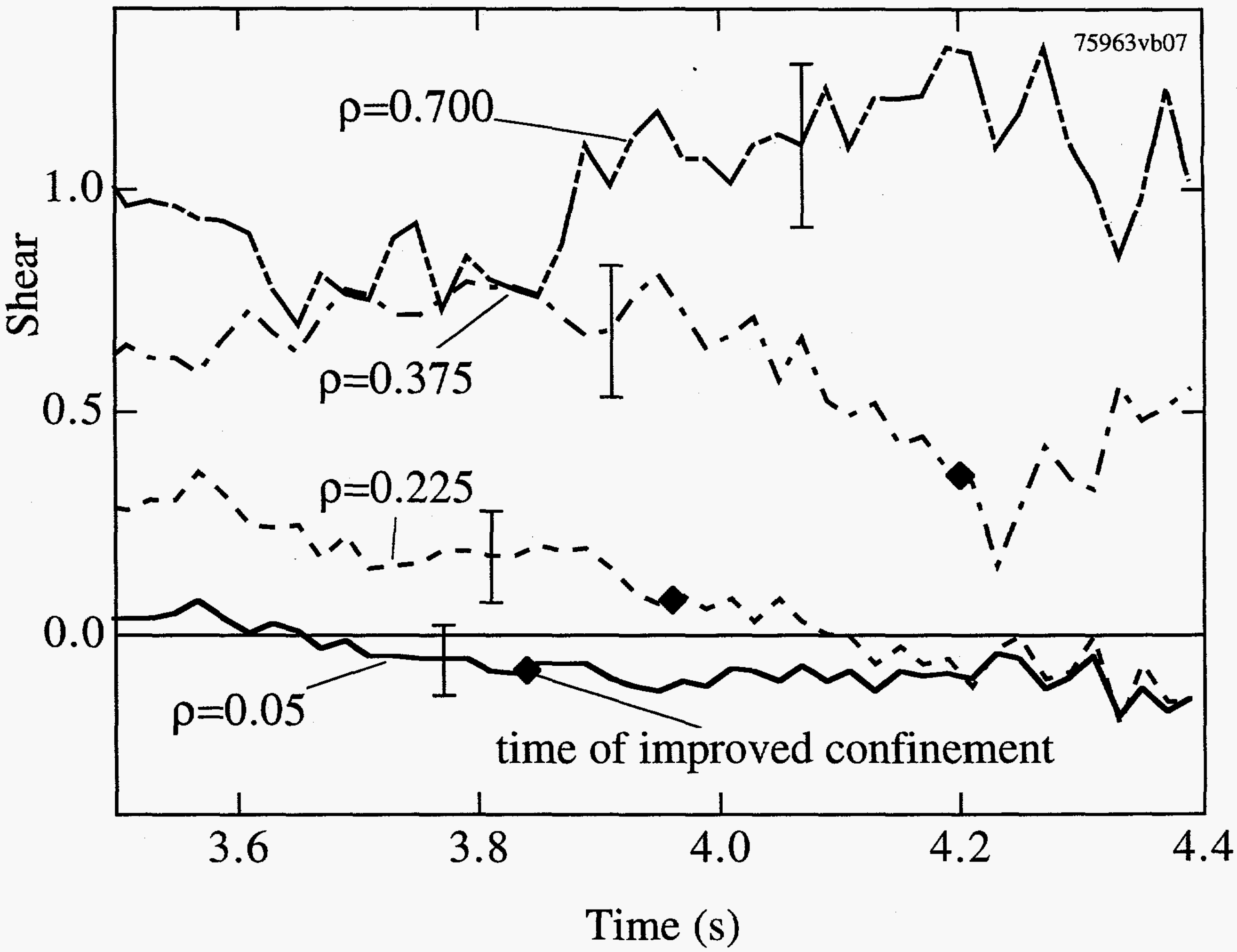
75963vb07
ρ=0.700
ρ=0.375
ρ=0.225
ρ=0.05
time of improved confinement
Shear
1.0
0.5
0.0
3.6
3.8
4.0
4.2
4.4
Time (s)

Figure 6.

EXTERNAL DISTRIBUTION IN ADDITION TO UC-420

Dr. F. Paoloni, Univ. of Wollongong, AUSTRALIA
Prof. R.C. Cross, Univ. of Sydney, AUSTRALIA
Plasma Research Lab., Australian Nat. Univ., AUSTRALIA
Prof. I.R. Jones, Flinders Univ, AUSTRALIA
Prof. F. Cap, Inst. for Theoretical Physics, AUSTRIA
Prof. M. Heindler, Institut für Theoretische Physik, AUSTRIA
Prof. M. Goossens, Astronomisch Instituut, BELGIUM
Ecole Royale Militaire, Lab. de Phy. Plasmas, BELGIUM
Commission-European, DG. XII-Fusion Prog., BELGIUM
Prof. R. Boucíqué, Rijksuniversiteit Gent, BELGIUM
Dr. P.H. Sakanaka, Instituto Fisica, BRAZIL
Prof. Dr. I.C. Nascimento, Instituto Fisica, Sao Paulo, BRAZIL
Instituto Nacional De Pesquisas Espaciais-INPE, BRAZIL
Documents Office, Atomic Energy of Canada Ltd., CANADA
Ms. M. Morin, CCFM/Tokamak de Varennes, CANADA
Dr. M.P. Bachynski, MPB Technologies, Inc., CANADA
Dr. H.M. Skarsgard, Univ. of Saskatchewan, CANADA
Prof. J. Teichmann, Univ. of Montreal, CANADA
Prof. S.R. Sreenivasan, Univ. of Calgary, CANADA
Prof. R. Marchand, INRS-Energie et Materiaux, CANADA
Dr. R. Bolton, Centre canadien de fusion magnétique, CANADA
Dr. C.R. James,, Univ. of Alberta, CANADA
Dr. P. Lukác, Komenského Universzita, CZECHO-SLOVAKIA
The Librarian, Culham Laboratory, ENGLAND
Library, R61, Rutherford Appleton Laboratory, ENGLAND
Mrs. S.A. Hutchinson, JET Library, ENGLAND
Dr. S.C. Sharma, Univ. of South Pacific, FIJI ISLANDS
P. Mähönen, Univ. of Helsinki, FINLAND
Prof. M.N. Bussac, Ecole Polytechnique,, FRANCE
C. Mouttet, Lab. de Physique des Milieux Ionisés, FRANCE
J. Radet, CEN/CADARACHE - Bat 506, FRANCE
Prof. E. Economou, Univ. of Crete, GREECE
Ms. C. Rinni, Univ. of Ioannina, GREECE
Preprint Library, Hungarian Academy of Sci., HUNGARY
Dr. B. DasGupta, Saha Inst. of Nuclear Physics, INDIA
Dr. P. Kaw, Inst. for Plasma Research, INDIA
Dr. P. Rosenau, Israel Inst. of Technology, ISRAEL
Librarian, International Center for Theo Physics, ITALY
Miss C. De Palo, Associazione EURATOM-ENEA , ITALY
Dr. G. Grosso, Istituto di Fisica del Plasma, ITALY
Prof. G. Rostangni, Istituto Gas Ionizzati Del Cnr, ITALY
Dr. H. Yamato, Toshiba Res & Devel Center, JAPAN
Prof. I. Kawakami, Hiroshima Univ., JAPAN
Prof. K. Nishikawa, Hiroshima Univ., JAPAN
Librarian, Naka Fusion Research Establishment, JAERI, JAPAN
Director, Japan Atomic Energy Research Inst., JAPAN
Prof. S. Itoh, Kyushu Univ., JAPAN
Research Info. Ctr., National Instit. for Fusion Science, JAPAN
Prof. S. Tanaka, Kyoto Univ., JAPAN
Library, Kyoto Univ., JAPAN
Prof. N. Inoue, Univ. of Tokyo, JAPAN
Secretary, Plasma Section, Electrotechnical Lab., JAPAN
Dr. O. Mitarai, Kumamoto Inst. of Technology, JAPAN
Dr. G.S. Lee, Korea Basic Sci. Ctr., KOREA
J. Hyeon-Sook, Korea Atomic Energy Research Inst., KOREA
D.I. Choi, The Korea Adv. Inst. of Sci. & Tech., KOREA
Leandro Melendez Lugo, Inst. Nac'l. de Inves. Nucl, MEXICO
Prof. B.S. Liley, Univ. of Waikato, NEW ZEALAND
Inst of Physics, Chinese Acad Sci PEOPLE'S REP. OF CHINA
Library, Inst. of Plasma Physics, PEOPLE'S REP. OF CHINA
Tsinghua Univ. Library, PEOPLE'S REPUBLIC OF CHINA
Z. Li, S.W. Inst Physics, PEOPLE'S REPUBLIC OF CHINA
Prof. J.A.C. Cabral, Instituto Superior Tecnico, PORTUGAL
Prof. M.A. Hellberg, Univ. of Natal, S. AFRICA
Prof. D.E. Kim, Pohang Inst. of Sci. & Tech., SO. KOREA
Prof. C.I.E.M.A.T, Fusion Division Library, SPAIN
Dr. L. Stenflo, Univ. of UMEA, SWEDEN
Library, Royal Inst. of Technology, SWEDEN
Prof. H. Wilhelmson, Chalmers Univ. of Tech., SWEDEN
Centre Phys. Des Plasmas, Ecole Polytech, SWITZERLAND
Bibliotheek, Inst. Voor Plasma-Fysica, THE NETHERLANDS
Asst. Prof. Dr. S. Cakir, Middle East Tech. Univ., TURKEY
Dr. V.A. Glukhikh,Sci. Res. Inst. Electrophys.I Apparatus, USSR
Dr. D.D. Ryutov, Siberian Branch of Academy of Sci., USSR
Dr. G.A. Eliseev, I.V. Kurchatov Inst., USSR
Librarian, The Ukr.SSR Academy of Sciences, USSR
Dr. L.M. Kovrizhnykh, Inst. of General Physics, USSR
Kernforschungsanlage GmbH, Zentralbibliothek, W. GERMANY
Bibliothek, Inst. Für Plasmaforschung, W. GERMANY
Prof. K. Schindler, Ruhr-Universität Bochum, W. GERMANY
Dr. F. Wagner, (ASDEX), Max-Planck-Institut, W. GERMANY
Librarian, Max-Planck-Institut, W. GERMANY